Biosensors and Bioelectronics 149 (2020) 111848

Contents lists available at ScienceDirect

Biosensors and Bioelectronics

journal homepage: http://www.elsevier.com/locate/bios

One DNA circle capture probe with multiple target recognition domains for simultaneous electrochemical detection of miRNA-21 and miRNA-155

Sai Xu, Yuanyuan Chang, Zhongyu Wu, Yunrui Li, Ruo Yuan **, Yaqin Chai *

Key Laboratory of Luminescent and Real-Time Analytical Chemistry (Southwest University), Ministry of Education, College of Chemistry and Chemical Engineering, Southwest University, Chongqing, 400715, PR China

ARTICLE INFO

Keywords:
tetrahedron DNA nanostructure
DNA circle capture probe
Mimetic proximity ligation assay
Multiple microRNAs detection
Electrochemical biosensor

ABSTRACT

In this work, a novel DNA circle capture probe with multiple target recognition domains was designed to develop an electrochemical biosensor for ultrasensitive detection of microRNA-21 (miRNA-21) and miRNA-155 simultaneously. The DNA circle capture probe was anchored at the top of the tetrahedron DNA nanostructure (TDN) to simultaneously recognize miRNA-21 and miRNA-155 through multiple target recognition domains under the assistance of Helper strands, which could trigger mimetic proximity ligation assay (mPLA) for capturing the beacons ferrocene (Fc)-A1 and methylene blue (MB)-A2 to achieve multiple miRNAs detection. In this way, the local reaction concentration could be enhanced and avoid the interference of various capture probes compared with the traditional multiplexed electrochemical biosensor with the use of different capture probes, resulting in the significantly improvement of detection sensitivity. As a result, this proposed biosensor showed wide linearity ranging from 0.1 fM to 10 nM with detection limits of miRNA-21 and miRNA-155 as 18.9 aM and 39.6 aM respectively, which also could be applied in the simultaneously detection of miRNA-21 and miRNA-155 from cancer cell lysates. The present strategy paved a new path in the design of capture probes for achieving more efficient and sensitive multiple biomarkers detections and possessed the potential applications in clinical diagnostic of diseases.

1. Introduction

MicroRNAs (miRNAs) was regard as tumor suppressors and oncogenes in cancers which was a kind of small noncoding RNAs (Anastasiadou et al., 2018.). Therefore, miRNA expression profiles could be used as effective biomarkers in early cancer diagnostic and prognostic process (Yu et al., 2019; Sierzega et al., 2017; Gao et al., 2018). In recent years, due to the convenient, sensitive, easy miniaturization, low cost of electrochemical biosensor, it was widely applied to miRNAs detection (Tavallaie et al., 2018; Guo et al., 2018; Liu et al., 2018). Usually, the developed electrochemical biosensor was designed to detect single miRNA, while evidences proved that a kind of disease may be closely associated with the simultaneous change of various miRNAs (Lu et al., 2005; El-Khazragy et al., 2019; Hu et al., 2018). Thus, the realization of multiple miRNAs simultaneous detection has a powerful predictive value in early diagnosis and prognosis of cancers. Recently, some of electrochemical biosensors were constructed to achieve simultaneous detection of multiple targets miRNAs by employing different single-stranded DNA (ssDNA) or hairpin as one-dimensional (1D) capture probes on the electrodes, which could obtain more accurate and detailed cancer information (Wegman and Krylov 2010; Yang et al., 2014; Wang et al., 2017). However, on account of the high surface disturbance and uncontrollable density of conventional 1D capture probes on the electrode, the accessibility of the molecules to capture probes decreased, suppressing the efficiency and sensitivity of multiple targets detection (Wen et al., 2011; Zhang et al., 2018; Li et al., 2018). In order to conquer the above mentioned predicaments of 1D capture probes, researchers have reported a tetrahedron DNA nanostructure (TDN) as three-dimensional (3D) nanostructure DNA capture probe for detecting miRNAs, which possessed well-controlled orientation, nanoscale distance and minimal nonspecific adsorption, significantly increasing the capture efficiency (Lin et al., 2015; He et al., 2018; Ma et al., 2019; Huang et al., 2018). But it was difficult to achieve multiple miRNAs detection due to the TDN only containing one vertex as capture probe which just have one target recognition domain to detect single miRNAs. Thus, it is urgently demand to innovate a novel DNA capture

* Corresponding author.
** Corresponding author.
E-mail addresses: yuanruo@swu.edu.cn (R. Yuan), yqchai@swu.edu.cn (Y. Chai).

https://doi.org/10.1016/j.bios.2019.111848
Received 14 August 2019; Received in revised form 23 October 2019; Accepted 2 November 2019
Available online 5 November 2019

probes with multiple target recognition domains combing with TDN to achieve simultaneous detection of multiple targets in one structure.

In recent years, DNA nanostructure plays a key role in nanoscience area on account of its flexibly programmable properties, high precision, and ease of preparation, which was extensively applied in the field of electrochemical biosensor (Wan et al., 2019; Yang et al., 2016; Lv et al., 2015). Thereinto, DNA circle has gathered great attentions owing to the inherent potential in less intertwine, switchable properties, favorable rigidity (Zhou et al., 2019; Centola et al., 2017). Recently, Hu and his coworkers depicted catalytic catenane by using two-circle interlocked DNA, which achieved the switch between two distinct DNAzymes through different ionic enzyme recognition region (Hu et al., 2015). However, it was incapable for catalytic catenane to synchronously realize two DNAzyme catalytic cleavage functions in one DNA structure. Thus, it is indispensable to design a novel DNA circle structure with multiple functions to achieve the simultaneous detection of multiple targets in one DNA structure. Here, a DNA circle capture probe with multiple target recognition domains was developed and applied in electrochemical biosensors for simultaneous multiple miRNAs detection, in which the capture probe could increase the local reaction concentration and improve the hybridization efficiency compared with those capture probes in traditional multiple targets detections. Furthermore, the TDN was used as a scaffold to immobilize the "bottom-up" DNA circle capture probe, further enhancing the uniformity of capture probe distribution on the electrodes to greatly enhance the detection sensitivity (Chen et al., 2019; Feng et al., 2017; Ge et al., 2014; Li et al., 2015; Lin et al., 2015).

In present work, with the use of a novel multifunctional DNA circle capture probe, an electrochemical biosensor was constructed and achieved highly sensitive and accurate miRNA-21 and miRNA-155 detection simultaneously. The working principle was illustrated in Scheme 1. First, the TDN was immobilized on the depAu/GCE surface through Au–N bond (Zhang et al., 2011; Zheng et al., 2016; Zhong et al., 2019). Then, the single strand chain at the top of TDN hybridized with the DNA circle capture probe which consisted of R and R1. Once targets miRNA-21 and miRNA-155 were introduced, the DNA circle capture probe with multiple target recognition domains could respectively capture miRNA-21 and miRNA-155 via the assistance of Helepr1 and Helper2 to trigger mimetic proximity ligation assay (mPLA), further capturing the Fc-labeled A1 and MB-labeled A2 to generate two electrical signal responses, realizing the fast multiple miRNAs detection in one DNA structure. And it was worth mentioning that this developed electrochemical biosensor was applied in the detection of miRNA-155 and miRNA-21 from cancer cell lysates. In addition, this proposed strategy also provided a unique avenue to design multifunctional capture probes for simultaneous multiple biomarkers detection.

2. Experiment section

2.1. Self-assembly of tetrahedron DNA nanostructure (TDN)

15 μL each strand, T1, T2, T3, and T4 (10 μM) were well-mixed with 40 μL TM buffer together. Then, heated the mixture about 10 min at 95 °C and subsequently cooled to 4 °C over 30 s. The final 100 μL TDN was successfully fabricated.

2.2. The fabrication of the biosensor

Firstly, 0.3 and 0.05 mm alumina slurry were used to polish the bare glassy carbon electrode (GCE) sequentially, and then the ultrasonic with ethanol and ultrapure water were utilized to gain mirror-like surface. Afterwards, in order to get a layer of gold nanoparticles (depAu), the electrode was put into $HAuCl_4$ (1%) solution to electrodeposit at −0.2 V for 30 s. Straight after, 10 μL of the abovementioned self-assembled TDN was dropped onto the depAu/GCE and interacted at room temperature for 16 h. At last, 10 μL mixture of 2.0 μM R and R1 was also dropwise added to the electrode surface (TDN/depAu/GCE) for 2 h at 37 °C. When the modified electrode (R-R1/TDN/depAu/GCE) was cleaned with PBS buffer, a novel multifunctional capture probe was established successfully.

2.3. Multiplexed detection of MicroRNAs

For the detection of the multiple targets, a mixture containing Helper1 and Helper2 of 2.0 μM, miRNA-21 and miRNA-155 of various concentrations were added onto the electrode (R-R1/TDN/depAu/GCE)

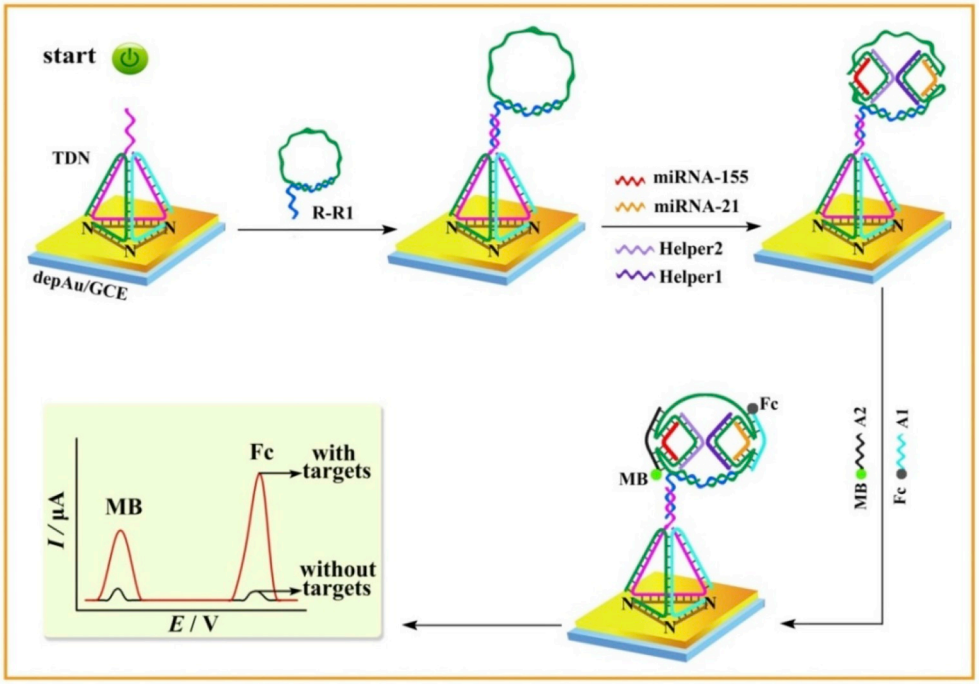

Scheme 1. Schematic illustration of the proposed biosensor for simultaneous detection of miRNA-21 and miRNA-155 via one novel DNA circle capture probe.

to react at 37 °C for 1 h. Since the electrode was washed with PBS buffer, DNA chains A1 (2.0 μM) and A2 (2.0 μM) were mixed together and then dropped onto the electrode surface for incubating 2 h at 37 °C. Finally, the signal responses were monitored by SWV in 0.1 M PBS.

2.4. Polyacrylamide-gel electrophoresis (PAGE)

First of all, DNA strands and DNA-loading buffer were mixed by volume ratio 5:1. Then, the samples were loaded onto the pre-made 16% polyacrylamide gel in 1 × TBE buffer (pH 8.0) for 120 min at 120 V.

3. Results and discussion

3.1. Polyacrylamide gel electrophoresis (PAGE) and atomic force microscopy (AFM) analysis

PAGE was employed to characterize the prepared TDN. As Fig. 1A showed, the bright bands of lane 1, lane 2, lane 3, lane 4 respectively corresponded to DNA strands T1, T2, T3, T4 (2 μM) and the highest band of TDN (2 μM) could be noticed (lane 5) with slowest migration for its large molecular weight. The positions of DNA strands in PAGE images were in accordance with DNA marker, suggesting the successful fabrication of TND. We also characterized the structure of TDN by AFM. As shown in Fig. 1B, the typically TDN morphology could be observed, which demonstrated the successful fabrication of TDN as well.

3.2. Electrochemical characterization of the biosensor

CV and EIS were tested in $[Fe(CN)_6]^{3-/4-}$ solution to characterize the immobilization procedure of this biosensor respectively. As shown in Fig. 2A, firstly, a couple of well-demarcated redox peaks of $[Fe(CN)_6]^{3-/4-}$ appeared distinctly for the bare GCE (curve a). After depAu was electrodeposited to the GCE, a marked increase of redox signal was obtained on account of the excellent conductivity of depAu (curve b). Subsequently, after the TDN was successful fixed on the electrode, the redox current dramatically reduced (curve c), because the DNA phosphate backbone with negative charge would repulse $[Fe(CN)_6]^{3-/4-}$. Afterwards, the subsequent addition of R-R1 caused an obviously inhibition of redox currents (curve d) attributing that the repulsion of $[Fe(CN)_6]^{3-/4-}$ and DNA was increased. Similarly, when Helper1 and Helper2 mixture was dropped onto the electrode, the redox currents also acquired a successive decrease (curve e).

We also used EIS to investigate the properties of the proposed electrode since the value of electron transfer resistance (R_{et}) value would change with the hinder of modified procedure on the electrode surface. As Fig. 2B displayed, the bare GCE with a small semicircle domain and a long tail showed a relatively low R_{et} and better conductivity (curve a). After depAu electrodeposited onto the electrode, a sharply decreased semicircle diameter (curve b) was obtained due to the excellent conductivity of depAu. Subsequently, R_{et} enhanced successively for TDN, R-R1, Helper1 and Helper2 incubated onto electrode stepwisely (curve c-e), which attributed to the increased repulsion from DNAs as well. The EIS results were in accordance with CV results which further demonstrated the biosensor was constructed with success.

3.3. Multiplex capability of the biosensor

The multiplex capability of this electrochemical biosensor was first investigated for miRNA-21 and miRNA-155 detection with the introduction of Helper1 and Helper2 simultaneously. The experiments were operated under optimized experimental conditions. No significant electrochemical response signal was observed for the blank test in Fig. 3A. In contrast, Fig. 3B exhibited a sharp current response at +0.46 V on account of the Fc labels was electrochemical oxidized in the existence of miRNA-21 (100 pM), while the peak current relating to MB at −0.31 V remained no change (Fig. 3B *vs.* A). Likewise, once miRNA-155 (100 pM) added, a remarkable electrochemical response signal was observed at −0.31 V, while the peak current at +0.46 V was not influenced as shown in Fig. 3C (Fig. 3C *vs.* A). These results suggested that the detection of only one target generated hardly impact on the detection of another target and further indicated the biosensor was capable of applying to the detection of either miRNA-21 or miRNA-155 reliably. Furthermore, once we applied a sample mixture of 100 pM miRNA-21 and miRNA-155 onto the electrode surface, as expected, two distinctly increased current responses at +0.46 V and −0.31 V were obtained, which corresponded to Fc and MB respectively (Fig. 3D), turning out the well feasibility of our biosensor for multiple miRNAs detection.

3.4. Analytical performance of the biosensor

MiRNA-21 and miRNA-155 of different concentrations were tested to inspect the analytical performance of this multiplexed electrochemical biosensor in the optimal experiment conditions. As Fig. 4A displayed, these pronounced current responses were observed with different concentrations of miRNAs. It generally revealed that the peak current responses which were related to the amounts of the redox tags would be significantly enlarged with the addition of the progressively increased concentrations of miRNAs. As displayed in Fig. 4B and C, the resulting calibration current plots manifested the linear relationships of the peak current response and the logarithm of miRNA-21 and miRNA-155 concentrations. With the increased concentrations of miRNAs (0.1 fM - 10 nM), the expression of regression equation was $I = 0.3255\ \lg c_{\text{miRNA-21}} + 6.3906$ and $I = 0.1894\ \lg c_{\text{miRNA-155}} + 3.6441$ with the correlation-coefficient value (R^2) was 0.9953 and 0.9984 respectively. The detection limits were calculated to be 18.9 aM and 39.6 aM respectively (Hua et al., 2019; Long and Winefordner 1983). As shown in Table S2, it was

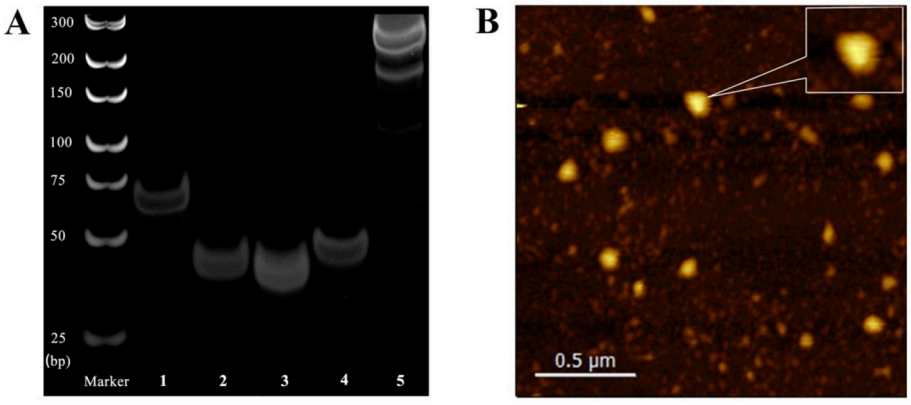

Fig. 1. (A) PAGE characterization analysis: lane 1, T1; lane 2, T2; lane 3, T3; lane 4, T4; lane 5, TDN; (B) AFM images of the structure of TDN.

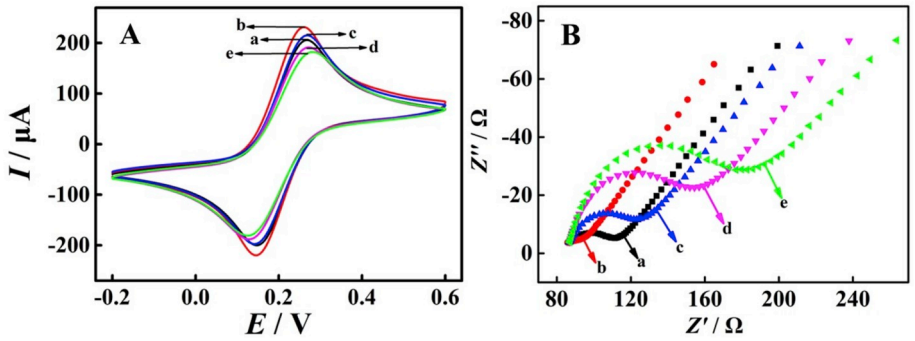

Fig. 2. (A) CV and (B) EIS responses of: (a) bare GCE; (b) depAu/GCE; (c) TDN/depAu/GCE; (d) R-R1/TDN/depAu/GCE; (e) Helper1+Helper2/R-R1/TDN/depAu/GCE.

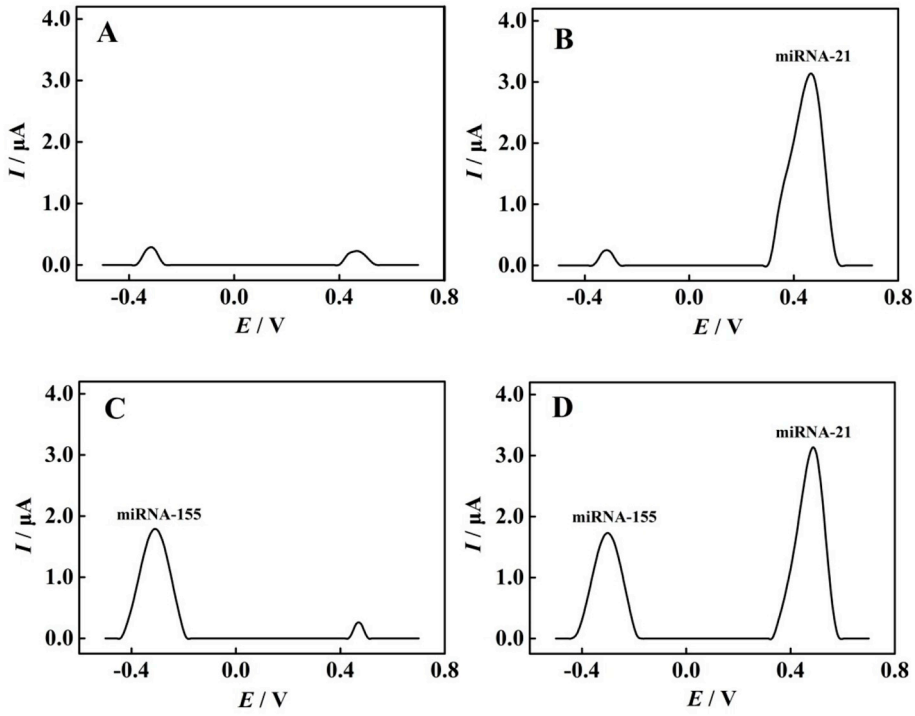

Fig. 3. SWV responses of the biosensors: (A) in the absence of miRNA-21 and miRNA-155; (B) in the presence of miRNA-21 and in the absence of miRNA-155; (C) in the absence of miRNA-21 and in the presence of miRNA-155; (D) in the presence of miRNA-21 and miRNA-155.

mentioning that this proposed biosensor possessed a relatively wider linear range and lower detection limits compared with other conventional biosensors, which attributed to the improved local reaction concentration and sensitivity of miRNAs detection.

3.5. Selectivity and application of the biosensor

In order to inspect the interference of the multiplexed electrochemical biosensor against other challenging molecules, we selected miRNA-141, miRNA-let-7a and miRNA-182-5p as interfering molecules. As Fig. 5A exhibited, there were negligible signal variations of miRNA-141, miRNA-let-7a and miRNA-182-5p compared to the blank even the concentration of interfering miRNAs as high as 10 nM. However, once a little amount of miRNA-21 and miRNA-155 (100 pM) were mixed with these interference miRNAs, the current response value rapidly increased and was immensely higher in contrast to the absence of targets, which implied a high selectivity of this multiplexed electrochemical biosensor toward miRNAs detection.

Moreover, we tested the application of the developed biosensor in real samples, miRNA-21 from cervical cancer cells (Hela) and miRNA-155 from human breast cancer cells (MCF-7) were put into practice. As Fig. 5B (b, c, d) displayed, in the monitor of samples containing lysates from Hela cells overexpressed miRNA-155and MCF-7 cells overexpressed miRNA-21 and miRNA-155, the current responses magnified with the cell numbers increased. These results were consistent with the former study, testifying that this multiplexed electrochemical biosensor achieved a good potential to monitor miRNAs from various cancer cells in early diagnostic.

4. Conclusion

In conclusion, by designing a novel DNA circle capture probe which was anchored at the top of TDN, an electrochemical biosensor was constructed for ultrasensitive detecting of miRNA-21 and miRNA-155 simultaneously. The DNA circle capture probe utilized TDN as a scaffold possessed controllable orientation, nanoscale distance and higher stability, which enhanced the sensitivity and decreased the detection limit of multiple miRNAs detection. Moreover, the novel DNA circle

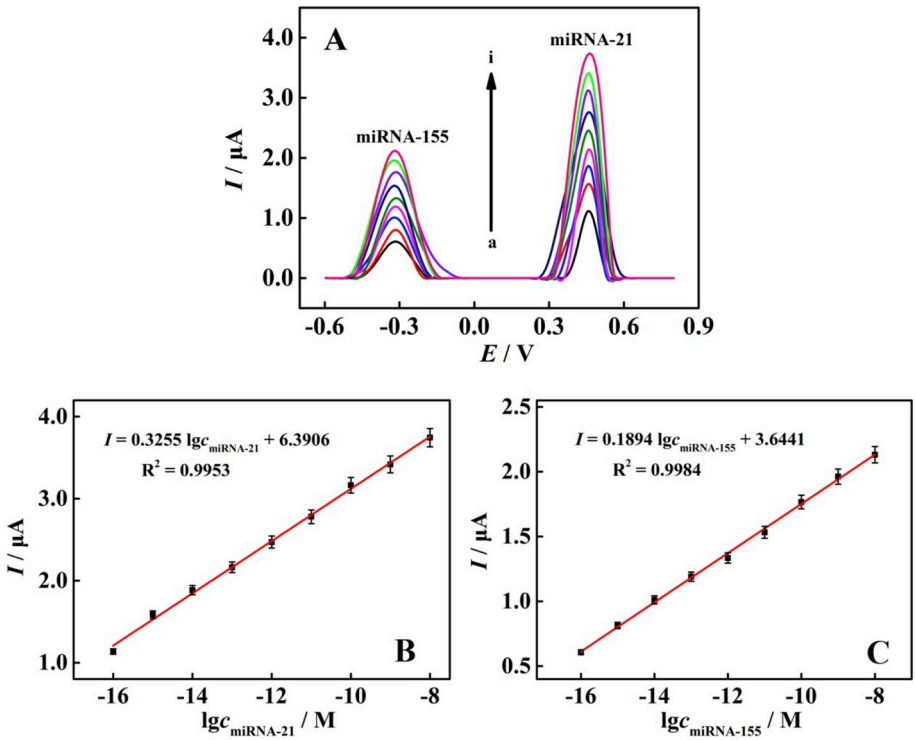

Fig. 4. (A) SWV responses for miRNA-21 and miRNA-155 simultaneous detection at: (a) 0.1 fM and 0.1 fM; (b) 1 fM and 1 fM; (c) 10 fM and 10 fM; (d) 100 fM and 100 fM; (e) 1 pM and 1 pM; (f) 10 pM and 10 pM; (g) 100 pM and 100 pM; (h) 1 nM and 1 nM; (i) 10 nM and 10 nM. (B and C) corresponding to the calibration plots of *I vs.* $lgc_{miRNA\text{-}21}$ and $lgc_{miRNA\text{-}155}$, respectively. Error bars, SD, n = 3.

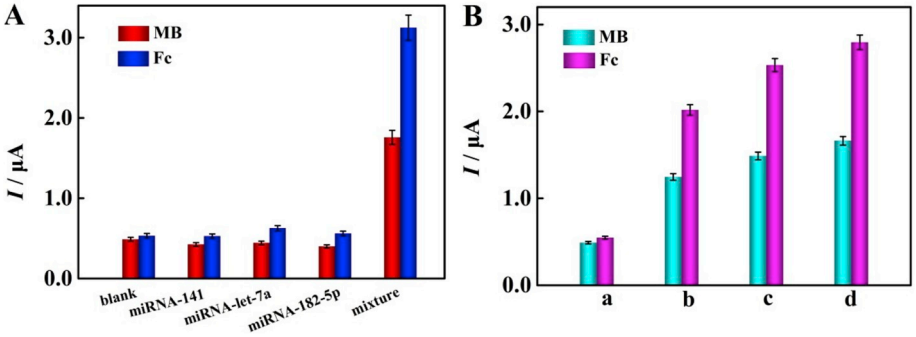

Fig. 5. (A) Specificity of the biosensor for miRNA-21 and miRNA-155 against other interfering miRNAs (10 nM); (B) The detection of miRNA-21 and miRNA-155 from Hela and MCF-7: (a) blank; (b) 10^2 cancer cells; (c) 10^3 cancer cells; (d) 10^4 cancer cells.

capture probe possessed multiple target recognition domains to capture multiple miRNAs just in one DNA structure for increasing the local reaction concentration, resulting in the improvement of detection speed and efficiency. Overall, this strategy exploits a novel avenue in the design of multifunctional capture probe for multiplexed electrochemical biosensor and also has the potential applications in early cancer diagnostic.

Declaration of competing interest

The authors declare that they have no known competing financial interests or personal relationships that could have appeared to influence the work reported in this paper.

CRediT authorship contribution statement

Sai Xu: Conceptualization, Data curation, Formal analysis, Investigation, Writing - original draft, Writing - review & editing. **Yuanyuan Chang:** Conceptualization, Writing - original draft, Supervision. **Zhongyu Wu:** Data curation, Investigation. **Yunrui Li:** Conceptualization, Writing - original draft, Supervision. **Ruo Yuan:** Funding acquisition, Resources, Project administration, Supervision. **Yaqin Chai:** Funding acquisition, Resources, Writing - review & editing.

Acknowledgements

This paper was financially supported by the National Natural Science Foundation of China (21675129, 21775124 and 21575116) and the Fundamental Research Funds for the Central Universities (XDJK2018AA003), China.

Appendix A. Supplementary data

Supplementary data to this article can be found online at https://doi.org/10.1016/j.bios.2019.111848.

References

Anastasiadou, E., Jacob, L.S., Slack, F.J., 2018. Nat. Rev. Cancer 18, 5–18.
Centola, M., Valero, J., Famulok, M., 2017. J. Am. Chem. Soc. 139, 16044–16047.
Chen, X., Huang, J., Zhang, S., Mo, F., Su, S.S., Li, Y., Fang, L.C., Deng, J., Huang, H., Luo, Z.X., Zheng, J.S., 2019. ACS Appl. Mater. Interfaces 11, 3745–3752.
El-Khazragy, N., Noshi, M.A., Abdel-Malak, C., Zahran, R.F., Swellam, M., 2019. J. Cell. Biochem. 120, 6315–6321.
Feng, Q.M., Zhou, Z., Li, M.X., Zhao, W., Xu, J.J., Chen, H.Y., 2017. Biosens. Bioelectron. 90, 251–257.
Gao, C.D., Zhou, C., Zhuang, J., Liu, L.J., Liu, C., Li, H.Y., Liu, G.X., Wei, J.Y., Sun, C.G., 2018. J. Cell. Biochem. 119, 7080–7090.
Ge, Z.L., Lin, M.H., Wang, P., Pei, H., Yan, J., Shi, J.Y., Huang, Q., He, D.N., Fan, C.H., Zuo, X.L., 2014. Anal. Chem. 86, 2124–2130.
Guo, J., Yuan, C.J., Yan, Q., Duan, Q.Y., Li, X.L., Yi, G., 2018. Biosens. Bioelectron. 105, 103–108.
He, L., Lu, D.Q., Liang, H., Xie, S.T., Zhang, X.B., Liu, Q.L., Yuan, Q., 2018. J. Am. Chem. Soc. 140, 258–263.
Huang, R.R., He, N.Y., Li, Z.Y., 2018. Biosens. Bioelectron. 109, 27–34.
Hua, X.Y., Yang, E.F., Yang, W.T., Yuan, R., Xu, W.J., 2019. Chem. Commun. 55, 12463–12466.
Hu, J., Liu, M.H., Zhang, C.Y., 2018. Chem. Sci. 9, 4258–4267.
Hu, L.Z., Lu, C.H., Willner, I., 2015. Nano Lett. 15, 2099–2103.
Li, C., Hu, X.L., Lu, J.Y., Mao, X.X., Xiang, Y., Shu, Y.Q., Li, G.Q., 2018. Chem. Sci. 9, 979–984.
Lin, M.H., Wang, J.J., Zhou, G.B., Wang, J.B., Wu, N., Lu, J.X., Gao, J.M., Chen, X.Q., Shi, J.Y., Zuo, X.L., Fan, C.H., 2015. Angew. Chem. 127, 2179–2183.
Liu, S.H., Yang, Z.H., Chang, Y.Y., Chai, Y.Q., Yuan, R., 2018. Biosens. Bioelectron. 119, 170–175.
Li, Y., Wen, Y.L., Wang, L.L., Liang, W., Xu, L., Ren, S.Z., Zou, Z.Y., Zuo, X.L., Fan, C.H., Huang, Q., Liu, G., Jia, N.Q., 2015. Biosens. Bioelectron. 67, 364–369.
Long, G.L., Winefordner, J.D., 1983. Anal. Chem. 55, 712A–724A.
Lu, J., Getz, G., Miska, E.A., Alvarez-Saavedra, E., Lamb, J., Peck, D., Sweet-Cordero, A., Ebert, B.L., Mak, R.H., Ferrando, A.A., Downing, J.R., Jacks, T., Horvitz, H.R., Golub, T.R., 2005. Nature 435, 834–838.
Lv, Y.F., Hu, R., Zhu, G.Z., Zhang, X.B., Mei, L., Liu, Q.L., Qiu, L.P., Wu, C.C., Tan, W.H., 2015. Nat. Protoc. 10, 1508–1524.
Ma, J.H., Xue, L., Zhang, M.L., Li, C., Xiang, Y., Liu, P., Li, G.X., 2019. Biosens. Bioelectron. 127, 194–199.
Sierzega, M., Kaczor, M., Kolodziejczyk, P., Kulig, J., Sanak, M., Richter, P., 2017. Br. J. Canc. 117, 266–273.
Tavallaie, R., McCarroll, J., Grand, M.L., Ariotti, N., Schuhmann, W., Bakker, E., Tilley, R.D., Hibbert, D.B., Kavallaris, M., Gooding, J.J., 2018. Nat. Nanotechnol. 13, 1066–1071.
Wang, J.R., Lu, Z.X., Tang, H.L., Wu, L., Wang, Z.X., Wu, M.H., Yi, X.Y., Wang, J.X., 2017. Anal. Chem. 89, 10834–10840.
Wan, Y., Zhu, N.H., Lu, Y., Wong, P.K., 2019. Anal. Chem. 91, 2626–2633.
Wegman, D.W., Krylov, S.N., 2010. Angew. Chem. Int. Ed. 50, 10335–10339.
Wen, Y.L., Pei, H., Wan, Y., Su, Y., Huang, Q., Song, S.P., Fan, C.H., 2011. Anal. Chem. 83, 7418–7423.
Yang, C.Y., Dou, B.T., Shi, K., Chai, Y.Q., Xiang, Y., Yuan, R., 2014. Anal. Chem. 86, 11913–11918.
Yang, X.L., Tang, Y.N., Mason, S.D., Chen, J.B., Li, F., 2016. ACS Nano 10, 2324–2330.
Yu, H.X., Guan, Z., Cuk, K., Zhang, Y., Breneer, H., 2019. Cancers 11, 415.
Zhang, X.L., Yang, Z.H., Chang, Y.Y., Qing, M., Yuan, R., Chai, Y.Q., 2018. Anal. Chem. 90, 9538–9544.
Zhang, T., Yang, Z.Q., Liu, D.S., 2011. Nanoscale 3, 4015–4021.
Zheng, Y.N., Liang, W.B., Xiong, C.Y., Yuan, Y.L., Chai, Y.Q., Yuan, R., 2016. Anal. Chem. 88, 8698–8705.
Zhong, H.T., Yu, C., Gao, R.F., Chen, J., Yu, Y.J., Geng, Y.Q., Wen, Y.L., He, J.L., 2019. Biosens. Bioelectron. 144, 111635.
Zhou, W.J., Li, D.X., Yuan, R., Xiang, Y., 2019. Anal. Chem. 91, 3628–3635.